A Theoretical and Experimental Study of Filler Effect on Stress-Deformation-Segmental Orientation Relations for Poly(dimethylsiloxane) Networks

Liliane Bokobza

Laboratoire de Physico-Chimie Structurale et Macromoleculaire, ESPCI, 10 rue Vauquelin, 75231 Paris, Cedex 05, France

Burak Erman*

Faculty of Engineering and Natural Sciences, Sabanci University, Tuzla, 81474, Istanbul, Turkey

Received February 11, 2000; Revised Manuscript Received July 3, 2000

ABSTRACT: Results of stress−strain, infrared dichroism, and birefringence experiments on silica-filled poly(dimethylsiloxane) networks show strong upturns of the stress with increasing deformation while segmental-orientation-strain relations remain linear over the same deformation range. As a result of this difference, the stress−optical coefficient exhibits an unusual dependence on deformation. The upturn in the stress results from the limited extensibility of the chains, inferred from the upturns in the Mooney−Rivlin plots presented. To explain these observations from a molecular perspective, we characterized the end-to-end distributions of different length poly(dimethylsiloxane) chains by Monte Carlo isomeric state calculations and derived stress-deformation-orientation relations for networks made of these chains by employing the three-chain network model. The results of the molecular model, in parallel with experimental observation, show strong differences between stress and orientation behavior.

Introduction

Recent results on poly(dimethylsiloxane) (PDMS) networks[1] filled with various amounts of silica particles have shown that reinforcement increases the modulus of elasticity significantly while it causes only a moderate increase in segmental orientation. This observation is apparently controversial when the results are interpreted in terms of unfilled Gaussian networks where the ratio of segmental orientation to stress is constant at all levels of strain. The constancy of the stress optical coefficient is well documented in experimental studies of Gaussian networks.[2,3] The observed differences between stress and orientation in filled networks result from finite chain extensibility. Especially at higher degrees of reinforcement, short chains bridging neighboring filler particles contribute to the modulus significantly. This is because short chains readily reach their maximum lengths, after which larger forces are needed to change the bond angles and bond lengths. The orientation, on the other hand, increases as long as the chain configurations are modified and the bonds are reoriented with increasing end-to-end distance. At the limit of maximum extensibility, no further reorientation of segments is possible, other than orientation resulting from bond angle and bond length changes, which are of secondary importance.

The specific aim of the present work is to provide a statistical mechanical explanation of the effects of finite chain extensibility on stress and orientation and to provide experimental evidence in support of the molecular interpretation. Calculations are based on the rotational isomeric state model of PDMS chains, according to which various conformations are generated by the conditional Monte Carlo technique, and the end-to-end distribution, force, and segmental orientation are calculated. Such calculations have previously been employed for obtaining the force−deformation relations and segmental orientation-deformation relations[3−5] for PDMS. Our theoretical treatment is based on the three-chain model of a network, originally applied to PDMS chains by Mark and Curro.[4] The experimental work is performed on randomly cross-linked PDMS chains in the presence of silica fillers. Segmental orientation is determined by infrared and, independently by birefringence measurements.

* Corresponding author. E-mail: erman@sabanciuniv.edu.

Stress-Deformation-Segmental Orientation Relations for Elastomers: The Three-Chain Approximation

The change ΔA of the Helmholtz free energy of a deformed network may suitably be approximated as the sum of changes of the free energies of chains in three coordinate directions

$$\Delta A = (\nu/3)(\Delta A_x + \Delta A_y + \Delta A_z) \qquad (1)$$

where ΔA_i is the change in the free energy of a single chain directed along the ith coordinate axis. This expression forms the basis of the three-chain model of Treloar.[6] The model assumes that a third of the ν network chains extend along each of the three coordinate directions. The free energy of a chain kept at a fixed end-to-end distance r is related to the probability density of r by the relation[7]

$$\Delta A = c(T) - kT \ln P(r) \qquad (2)$$

where k is the Boltzmann constant and $c(T)$ is a function of temperature, T. For a network of ν chains, the elastic free energy of the network in uniaxial tension is

10.1021/ma000261t CCC: $19.00
Published on Web 10/25/2000

obtained from eqs 1 and 2 as[6]

$$\Delta A_{el} = -\frac{\upsilon kT}{3}\left[\ln\frac{P(\alpha r_0)}{P(r_0)} + 2\ln\frac{P(\alpha^{-1/2} r_0)}{P(r_0)}\right] \quad (3)$$

Here, r_0 is the root-mean square end-to-end vector, $\langle r^2\rangle_0^{1/2}$, of unperturbed chains, and α is the extension ratio, defined as the length of the deformed network divided by the undeformed length. The probability density function $P(r)$ and the radial distribution function $W(r)$ are related by

$$W(r) = 4\pi r^2 P(r) \quad (4)$$

The radial distribution function $W(r)$ easily lends itself to computation by techniques such as the rotational isomeric state formalism or the Monte Carlo simulation technique. This is especially important for chains which are relatively short and not close to their Gaussian limits. The three-chain model allows the incorporation of the chemical specificity and the finite size effects of chains into a network model. The stress-deformation relations for networks with short PDMS chains have previously been studied with the three-network model by Mark and Curro.[4] The treatment of stress-deformation and the extension to segmental orientation of the present paper is based on this reference.

The true stress, t, in simple tension, defined as the ratio of the force to the deformed cross-sectional area, is obtained form eq 3 by using the thermodynamic relation $t = \alpha/V_0(\partial\Delta A_{el}/\partial\alpha)_T$ as

$$t = -\frac{\upsilon kT}{3V_0}\left[\alpha\frac{\partial \ln P(\alpha r_0)}{\partial\alpha} - \alpha^{-3/2}\frac{\partial \ln P(\alpha^{-1/2} r_0)}{\partial\alpha^{-1/2}}\right] \quad (5)$$

where V_0 is the volume of network in the reference state where the root-mean-square chain length is r_0.

The three-chain network model represents the affine network model of rubber elasticity. In the remaining sections of the present paper, we choose the affine network model as our reference and treat the stress as well as orientations in terms of this model. Relationship of the affine network model to the phantom network model and more realistic constrained junction models is now well documented in the literature and may be consulted for a more detailed discussion of the effects of network topology on strain and orientation.[3]

The three-chain model may be extended to explain segmental orientation in deformed networks. The second Legendre polynomial P_2 representing segmental orientation for a chain with its two ends fixed at a separation of r is

$$P_2(r) = \frac{3}{2}\left(\langle\cos^2\theta\rangle_r - \frac{1}{3}\right) \quad (6)$$

where θ is the angle between the direction of stretch and a characteristic local axis of the chain, whose orientation is being investigated. The left-hand-side of eq 6 represents an average over all configurations of the chain subject to the constraint that the end-to-end vector is kept fixed at **r**. Equation 6 may be used to perform the averaging over the distribution of chains of the three network model. Orientation measurements in uniaxial stretch observe the differences between chains along the direction of stretch and chains in the lateral direction.

Table 1. Some Values of Interest for the PDMS Chains[a]

property	$n = 20$	$n = 30$	$n = 100$
r_{max}	29.0	43.5	145.0
$r_0 = \langle r^2_0\rangle^{1/2}$	17.3	21.5	42.6
D_0 (from Nagai expression[5])	0.064	0.056	0.013
D_0 (this work)	0.175	0.100	0.022

[a] l = bond length = 1.64.

Thus

$$P_2(\alpha) = \int_0^\infty [\alpha^{-1}P(\alpha^{-1}r)P_2(r) - \alpha^{1/2}P(\alpha^{1/2}r)P_2(r)]\,dr$$
$$= \overline{P_2(\alpha r)} - \overline{P_2(\alpha^{-1/2}r)} \quad (7)$$

Here, the overbars denote averaging over all chains in the distribution.

Results of Monte Carlo Calculations for PDMS chains

In this section, we calculate the radial distribution functions for PDMS chains having 20, 30, and 100 repeat units, and use eqs 4, 5, and 7 to characterize the stress and segmental orientation in networks of PDMS having chains of these lengths.

The structure and energy parameters of PDMS chains provided by Besbes et al.[5] are used. The reader is referred to this paper for details of the data and calculations. The number n of bonds of each chain is identified with the number of Si−O bonds, for $n = 20$, 30, and 100. These values of n are representative for the three different regimes of chain lengths in PDMS chains. The chain with $n = 20$ represents a short chain, the one with $n = 100$ represents a chain that have reached the Gaussian limit, and the one with $n = 30$ is intermediate between a short and a long chain. For each n, 10 000 configurations are generated according to the conditional Monte Carlo (MC) technique.[4,5] Some average values of interest for the chains are presented in Table 1. All calculations are performed at 27 °C. The values of r_{max} have been calculated by assuming an all-trans configuration. It is to be noted, however, that due to the differences of consequtive bond angles along the chain, the all-trans form of the PDMS chain does not lie along a straight line. r_{max} in the present calculations is obtained from the vector that connects the two ends of the chain.

The radial distribution function is obtained by calculating the number of configurations for which the end-to-end vector has the scalar value of r, irrespective of its direction. The interval $0 \le r/nl \le 1.0$ is divided into 20 bins of width 0.05, and the number of chains having r values falling into each bin is determined. The dependence of $W(r)$ on r is shown in Figure 1 for $n =$ 20, 30, and 100. The curves are normalized such that the area enclosed under each curve is unity. The curve for $n = 20$ exhibits the characteristic feature that the peak is skewed toward higher r and that it abruptly terminates at higher values of r. This is one indication of the non-Gaussian feature of the short chains. The curve for $n = 30$ exhibits the same features but to a lesser extent. The curve for $n = 100$ appears similar to a Gaussian curve, but it also terminates at a finite r. It is to be noted that termination of a distribution function at a finite r always results in an upturn of the force−extension relation irrespective of the number of repeat units in the chain.

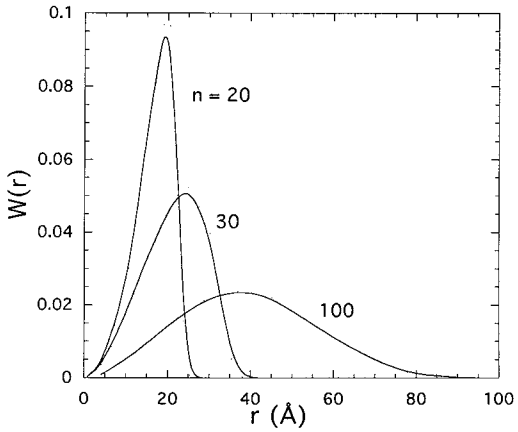

Figure 1. The dependence of $W(r)$ on r, for $n = 20$, 30, and 100. The area enclosed under each curve is normalized to unity.

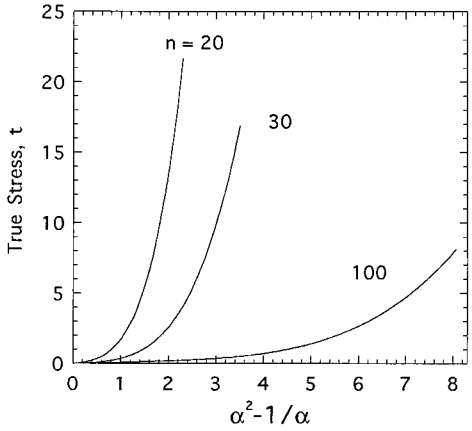

Figure 2. Results for the true stress as a function of the strain function, $\alpha^2 - 1/\alpha$, for $n = 20$, 30 and 100.

The expressions for $P(r)$, obtained from $W(r)$ by the use of eq 4 is expressed as a fourth-order polynomial in r. The expressions for the true stress in simple tension for three monodisperse networks with chains of $n = 20$, 30, and 100 are obtained by using eq 5. The fourth-order polynomial expressions are used for the differentiations. Results for the true stress are presented in Figure 2 as a function of the strain function, $\alpha^2 - 1/\alpha$. The curves are terminated at extensions at which the value of $r = \alpha r_0$ reached the zero probability regions shown in Figure 1. The tangent of a curve at a given value of the strain function represents the modulus of the network. The curves for the two networks with $n = 20$ and 30 exhibit strong upturns at extensions approaching full extension, indicating that the modulus increases significantly with extension. The curve for $n = 100$ also exhibits an upturn, but at very large values of the strain. The upturn corresponds to r values at the tail of the corresponding curve in Figure 1 where departure from a Gaussian is larger.

Calculations of the orientation are made for vectors along the O−O bonds of the PDMS chains. These are the vectors whose orientations are observed in the experiments which are reported in detail below. The mean orientations of all the O−O bonds along the chain are considered.[5] The value of $\cos^2 \theta$ is obtained for all of the 20 bins in the MC simulations. Calculations of $P_2(\alpha)$ are made according to eq 7. The values of $P_2(r)$ obtained from MC simulations are expressed as fourth-order polynomial functions of r. These functions are

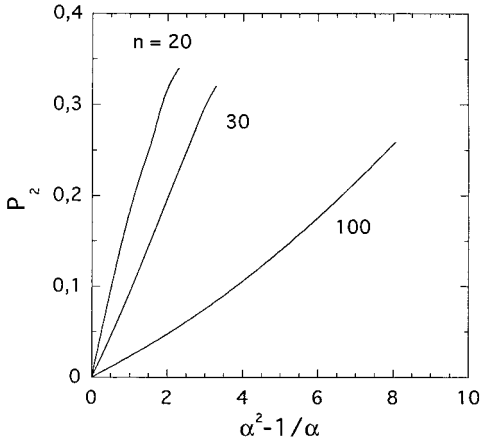

Figure 3. Calculated values of segmental orientation, P_2, as a function of the strain function for $n = 20$, 30 and 100.

inserted into the integrand in eq 7. Results of calculations are presented in Figure 3, where P_2 values are plotted as a function of the strain function for $n = 20$, 30, and 100. Unlike the true stress vs strain curves, the orientation curves do not exhibit the upturn at high extensions.

The D_0 values obtained by fitting least-squares lines to the initial portions of the curves are presented in Table 1. It is to be noted that the values of D_0 obtained in this manner are larger than those obtained by the Nagai expression[5]

$$D_0 = \frac{1}{10}\left[3\frac{\langle r^2 \cos^2 \Phi\rangle_0}{\langle r^2\rangle_0} - 1\right] \qquad (8)$$

which is based on the long chain limit assumption. Here, Φ is the angle between the vector whose orientation is being considered and the end-to-end vector. The discrepancy diminishes with increasing chain length, however.

The ratio of the segmental orientation function to the true stress is proportional to the stress−optical coefficient of the network. The latter is defined as the ratio of the birefringence to true stress. For affine and phantom network models, the stress optical coefficient is independent of deformation. Birefringence experiments on networks with sufficiently high molecular weight chains indeed lead to stress optical coefficients which are independent of strain, as shown, for example for an unfilled network in the inset of Figure 9b below.[6,8] The results of the present calculations on non-Gaussian chains, on the other hand, exhibit strong dependence of the ratio on deformation. Results of calculations are presented in Figure 4, where the orientation function is plotted along the ordinate and the true stress along the abscissa. The curves for $n = 20$ and 30 are similar. The curve for $n = 100$ deviates somewhat from the two others, but is still nonlinear.

Stress and Segmental Orientation Experiments on Filled PDMS Networks

In the following sections, we report results of stress-deformation and segmental orientation experiments on filled PDMS samples. The elastic properties of filled systems are affected by the presence of short chains connecting the filler particles, which consequently induce larger molecular deformations. The results to be reported below indeed show the signature of finite

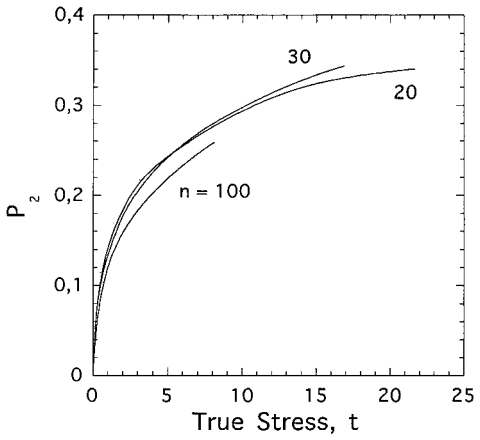

Figure 4. Orientation function plotted against the true stress.

extensibility, similar to those observed for short chains in the Monte Carlo calculations reported above. And, strikingly, while significant upturns take place in the stress−strain curves, no upturn is observed in orientation−strain relations.

Samples. Pyrogenic silica is blended with poly(dimethylsiloxane)chains containing a small amount of vinyl side groups (0.078%) in order to carry out a peroxide-cure. The amount of vinyl groups determine the molecular weight between cross-links, M_c, estimated to be about 17 300 for the unfilled sample. The filled sample studied here contains 40 phr (parts of silica per hundred parts of rubber, by weight) of treated silica (specific surface area of 300 $m^2\ g^{-1}$) which has been previously treated to deactivate part of the reactive groups on the particle surface, to reduce interactions between particles and the matrix and between particles themselves too, thus improving the dispersion of the filler in the elastomer. The mode of interaction between the silica and the matrix is supposed to be through the remaining silanol groups present on the silica surface. Several other networks with differing filler contents were also investigated, but only the results of the 40 phr sample, chosen as the representative sample, are presented. More detailed information on experimental data is given in ref 1.

Stress−Strain Experiments. Stress−strain measurements were carried out by simply stretching strips of 40 × 10 × 0.2 mm^3 between two clamps by means of a sequence of increasing weights attached to the lower clamp. The distance between two marks was measured with a cathetometer after allowing sufficient time for equilibration. All experiments were performed at room temperature.

Infrared Measurements. Infrared spectra were recorded with an FTIR spectrometer (Nicolet model 210) with a resolution of 4 cm^{-1} and an accumulation of 32 scans. The absorption A of infrared radiation is caused by the interaction of the electric field vector E of the incident light with the electric dipole-transition moment M associated with a particular molecular vibration:

$$A \propto (\vec{M} \cdot \vec{E})^2 \tag{9}$$

The effect of anisotropy of a selected absorption band of the infrared spectrum of the sample is reflected by the dichroic ratio R, defined as $R = A_{\parallel}/A_{\perp}$ ($A_{\parallel}$ and $A_{\perp}$ being the absorbances of the investigated band, measured with radiation polarized parallel and perpendicular to the stretching direction, respectively).

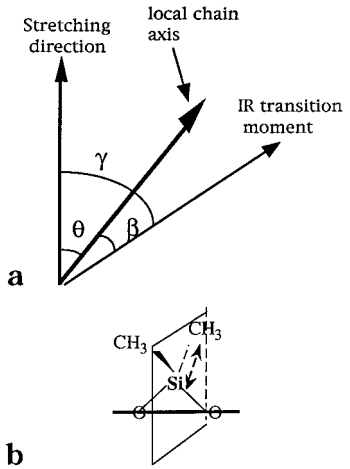

Figure 5. (a) Directions of the local chain axis (β) and the transition moment (γ) with respect to the direction of stretch. In the calculations, the local chain axis is taken as the vector joining two successive oxygen atoms along the chain backbone. Figure 5. (b) The local geometry of the PDMS chain, showing the two CH_3 units relative to the chain axis.

The orientation function $\langle P_2(\cos\theta)\rangle$ given by eq 6 is related to the measured dichroic ratio R by the expression[9,10]

$$\langle P_2(\cos\theta)\rangle = \frac{2}{(3\cos^2\beta - 1)} \cdot \frac{(R-1)}{(R+2)} = \frac{\langle P_2(\cos\gamma)\rangle}{\langle P_2(\cos\beta)\rangle} \tag{10}$$

where β and γ are the angles between the transition moment and the local chain axis and between the transition moment and the direction of stretch, respectively. $(R-1)/(R+2)$ is the dichroic function which is equal to the orientation $\langle P_2(\cos\gamma)\rangle$ of the transition moment with respect to the direction of stretch, and $\langle P_2(\cos\beta)\rangle = (^1/_2)(3\cos^2\beta - 1)$ is the orientation function relating the transition moment vector of the vibrational mode considered to the local chain axis of the polymer as shown in Figure 5a. The dichroic function $\langle P_2(\cos\gamma)\rangle = (R-1)/(R+2)$ directly gives the orientation of the transition moment vector with respect the direction of stretch.

Quantitative determination of $\langle P_2(\cos\theta)\rangle$ by the infrared technique requires a precise knowledge of the respective transition moment direction relative to the chain axis, i.e., the angle β. That means that the investigated absorption bands must be well assigned to normal vibrations of specified atomic groups. Such an assignment can be achieved by making a normal-coordinate analysis or looking at deuteration effects or dichroic behavior, experimentally.

In previous studies, we have investigated the dichroic behaviors of the bands located at 2500 and 4164 cm^{-1} respectively, ascribed to the overtone of the CH_3 symmetrical bending vibration located at 1260 cm^{-1} and to a combination of the symmetrical stretching mode of the methyl group at about 2905 cm^{-1} with the symmetrical bending mode. The transition moment associated with both vibrational modes lies along the CH_3−Si bond, which is a symmetry axis of the methyl group.[11] As already mentioned, determination of the orientation function requires the definition of the angle β between the transition moment of the investigated band and a directional vector characteristic of a given chain segment. For the particular case of PDMS chains, the

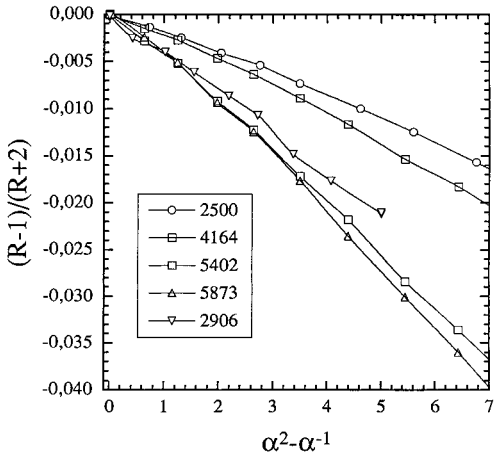

Figure 6. Dichroic functions $(R - 1)/(R + 2)$, plotted against the strain function $(\alpha^2 - \alpha^{-1})$ for different absorption bands located in the mid- as well as in the near-infrared region. The lines are interpolated through the experimental points to guide the eye.

chosen directional vector is that joining two successive oxygen atoms. The angle β is thus expected to be equal to 90°, as depicted in Figure 5b.

In addition to the analysis of the band located at 2500 cm^{-1}, we have also characterized bands between 4000 and 6000 cm^{-1} located in the near-infrared region (near-IR).[12] The near-infrared spectral region, which covers the interval between approximately 14000 and 4000 cm^{-1}, is dominated by absorption bands corresponding to overtones and combinations of fundamental C−H, O−H, and N−H vibrations, because of the large anharmonicity of those vibrations involving the light hydrogen atoms. As the overtones and combinations are much weaker than the fundamental absorption bands (usually by a factor of 10−100), one of the main advantage of near-IR spectroscopy is to allow the analysis of samples up to several millimeters thick.[12]

In Figure 6, dichroic functions $(R - 1)/(R + 2)$ are plotted against the strain function $(\alpha^2 - \alpha^{-1})$ for different absorption bands located in the mid-as well as in the near-infrared region. The lines are interpolated through the experimental points to guide the eye. The bands are related to vibrational modes belonging to the same symmetry species (irreducible representation A_1 of the C_{3v} point group of the methyl group). Consequently, the corresponding absorption bands are expected to exhibit the same dichroic behavior i.e., the same dichroic function.

This way of plotting the data arises from the proportionality between the orientation function and the dichroic function as given by the eq 10. On the other hand, plotting the dichroic function instead of $\langle P_2(\cos\theta)\rangle$ means that we are only looking at the orientation of the transition moment vectors with respect to the direction of stretch, without any assumption concerning the local chain axis defined by the angle β.

The results presented in Figure 6 show that the higher dichroic effect is obtained for the band at 5873 cm^{-1}. If we assume that the angle between the transition moment associated with this vibrational mode and the local chain axis has the highest value which is 90°, then we can estimate the angles β for the other modes. For the modes associated with the 2500 cm^{-1} band we find that $\beta \approx 65°$. The smaller value of β for this mode is most probably due to its being coupled with other vibrations. This result points out the main problem arising in the determination of molecular orientation by infrared dichroism and shows that near-infrared spectroscopy could be helpful for that purpose, since it allows the analysis of vibrational modes less coupled than those in the mid-infrared range.[13]

Birefringence. Measurements of strain birefringence of deformed networks is an alternative technique for determining the degree of orientation of chain segments. According to the theory, in an affine network model, the birefringence is related to the strain function by the expression[8,14]

$$\Delta n = \frac{\nu kTC}{V}(\alpha^2 - \alpha^{-1}) = D_1(\alpha^2 - \alpha^{-1}) \qquad (11)$$

where ν/V represents the number of chains per unit volume and C is the stress−optical coefficient which is related to the optical anisotropy Γ_2 of the network through the following equation:

$$C = \frac{2\pi(n^2 + 2)^2\Gamma_2}{27nkT} \qquad (12)$$

n is the mean refractive index. C is usually referred to in the literature as the stress−optical coefficient since

$$C = \Delta n/t \qquad (13)$$

The stress−optical coefficient was previously calculated for unfilled PDMS chains by using the rotational isomeric state formalism[8,14] to be 1.7×10^{-10} Pa^{-1}. From the present birefringence experiments we obtain the value of 1.5×10^{-10} Pa^{-1}, which is in agreement with the previous theoretical value. The relation between birefringence and the second-order moment of the orientation function is given by the expression

$$[\Delta n] = [\Delta n]_0 \langle P_2(\cos\theta)\rangle \qquad (14)$$

where $[\Delta n]_0$ is the intrinsic birefringence characteristic of the polymer.

$[\Delta n]_0$ may be called the maximum birefringence because the perfect orientation corresponds to $\langle P_2(\cos\theta)\rangle = 1$.

Results of Experiments

The results of stress-deformation experiments on filled and unfilled PDMS networks are presented in Figure 7, where the true stress is plotted as a function of the strain factor, $\alpha^2 - 1/\alpha$. The points represent experimental data. The lines through the points are drawn to guide the eye. The tangent of the curves indicate the modulus at the corresponding strain. The upturns in the curves indicate increase of the moduli with extension, similar to the corresponding curves obtained theoretically by the three-chain model of rubber elasticity.

In Figure 8, the orientation function determined by infrared dichroism measurements for networks with different amounts of fillers are presented as a function of the strain function. The effect of filler amount on segmental orientation is significant, as seen from the three curves. However, the dependence of the orientation function on the strain function remains a straight line for all levels of deformation. This observation is in agreement with the results of theoretical calculations.

In Figure 9a, the relationship between orientation and true stress is presented for the sample with 40 phr filler.

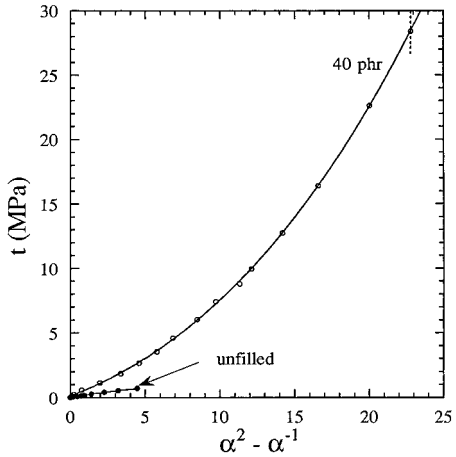

Figure 7. Results of stress−deformation experiments on filled and unfilled PDMS networks. The true stress is plotted as a function of the strain factor, $\alpha^2 - 1/\alpha$. The points represent experimental data. The lines through the points are drawn to guide the eye.

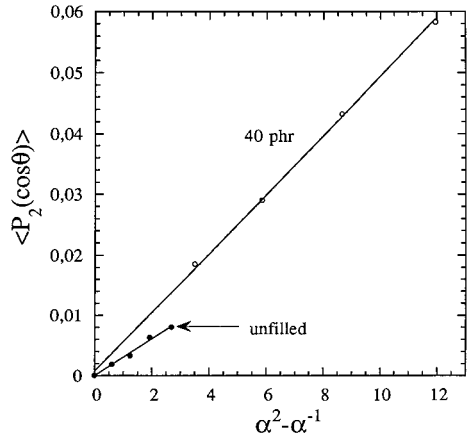

Figure 8. Orientation function determined by infrared dichroism measurements for networks with different amounts of fillers, presented as a function of the strain function.

Results from birefringence experiments are plotted in a similar way in Figure 9b. The points represent experimental data, and the curves through the points is the least-squares fourth-order curve. The slope of the orientation−stress diagram represents the stress optical coefficient of the system. For the typical unfilled elastomer, the stress optical coefficient is independent of the state of deformation, up to relatively high values of the latter. The inset in Figure 9b represents results of birefringence measurements on the unfilled sample, taken up to the rupture of the elastomer. The points are well represented by a straight line. The curves for the filled samples shown in Figure 9, parts a and b, exhibit pronounced departures from linearity at all levels of deformation. This indicates that the finite extensibility effect is observed in filled systems even at relatively small levels of macroscopic deformation.

Measurements of birefringence and infrared dichroism on samples containing different filler loadings showed that plots of Δn vs $\langle P_2 \rangle$ exhibited a single master curve. In a way this is surprising, because this indicates that infrared dichroism and birefringence are both only sensitive to the apparent molecular weight between cross-links.

In Figure 10, the reduced stress is presented as a function of inverse extension ratio for filled and unfilled

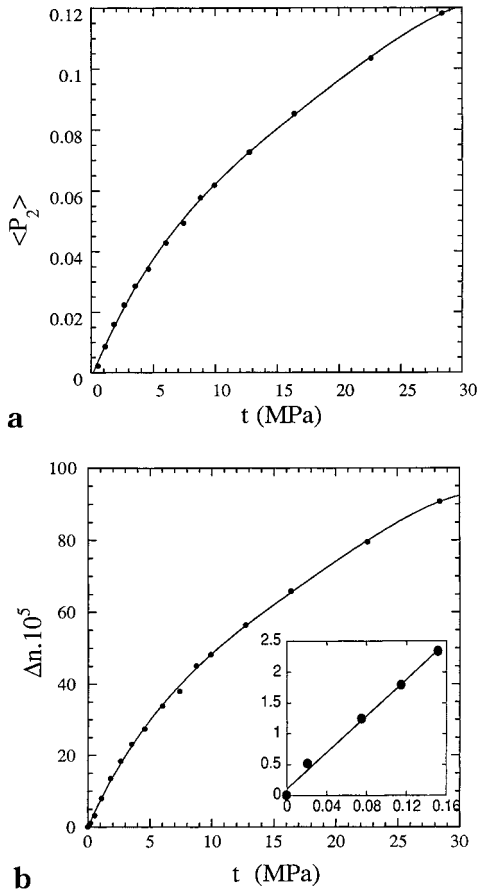

Figure 9. (a) Relationship between orientation and true stress obtained from infrared measurements. (b) Relationship between orientation and true stress obtained from infrared measurements. The points represent experimental data, and the curves through the points is the least-squares fourth-order curve.

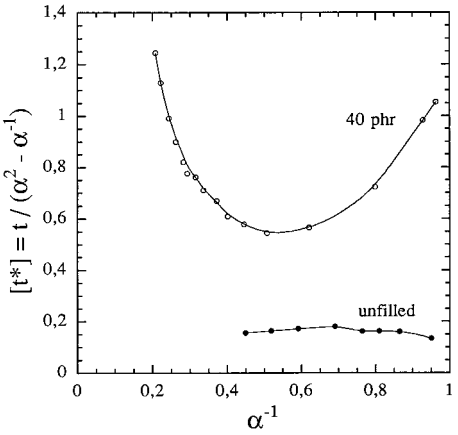

Figure 10. Reduced stress as a function of inverse extension ratio for filled and unfilled samples.

samples. The upturn at high deformations, which becomes more pronounced in samples with large amounts of filler, is typical of finite chain extensibility.

Conclusions

Simultaneous observation of stress and orientation in unfilled and filled elastomers, and the results of the related statistical mechanical model confirm that finite chain extensibility is the dominant factor affecting the unusual elastic properties of filled networks. This conclusion is based on the observation of steep upturns

in the stress−strain diagrams and the corresponding linearity of the orientation-strain diagrams. The obvious explanation of this observation is that when chains reach their finite extensibility limits, chain deformation and segmental orientation resulting from large-scale conformational rearrangements of chains stop although the applied force may be increased. The further increase of the force is taken up by the stiffer modes of deformation, i.e., bond length and bond angle changes. The latter modes of deformation do not result in large-scale changes in the end-to-end vectors of chains. The upturn of the Mooney−Rivlin plot seen in Figure 10 indeed indicates the finite extensibility effect in the filled system. The validity of this explanation is demonstrated by the statistical mechanical model, the results of which agree qualitatively with experimental observations. A more specific mode of analysis is possible with a more rigorous model of elasticity which considers randomly oriented chains in the undeformed network instead of the three chain model.

References and Notes

(1) Bokobza, L.; Monnerie, L. In *Chemical and Physical Networks, Formation and Control of Properties*; te Nijenhuis, K., Mijs, W. J., Eds.; Wiley: 1998; Vol. 1; p 321.

(2) Mark, J. E.; Erman, B. *Rubberlike Elasticity. A Molecular Primer*; Wiley-Interscience: New York, 1988.

(3) Erman, B.; Mark, J. E. *Structure and Properties of Rubberlike Materials*; Oxford University Press: Oxford, England, 1998.

(4) Mark, J. E.; Curro, J. G. *J. Chem. Phys* **1983**, *79*, 5705.

(5) Besbes, S.; Cermelli, I.; Bokobza, L.; Monnerie, L.; Bahar, I.; Erman, B.; Herz, J. *Macromolecules* **1992**, *25*, 1949.

(6) Treloar, L. R. G. *The Physics of Rubber Elasticity*, 3rd ed.; Oxford University Press: Clarendon, England, 1975.

(7) Flory, P. J. *Proc. R. Soc. London, A* **1976**, *351*, 351.

(8) Erman, B.; Flory, P. J. *Macromolecules* **1983**, *16*, 1601.

(9) Jasse, B.; Koenig, J. L. *J. Macromol. Sci., Rev. Macromol. Chem.* **1979**, *C17*, 61.

(10) Bokobza, L.; Amram, B.; Monnerie, L. In *Elastomeric Polymer Networks*; Mark, J. E., Erman, B., Ed.; Prentice Hall: Englewood Cliffs, NJ, 1992; pp 289−301.

(11) Buffeteau, T.; Desbat, B.; Bokobza, L. *Polymer* **1995**, *36*, 4339.

(12) Bokobza, L. *J. Near Infrared Spectrosc.* **1998**, *6*, 3.

(13) Bokobza, L.; Buffeteau, T.; Desbat, B. *Appl. Spectrosc.*, in press.

(14) Erman, B.; Flory, P. J. *Macromolecules* **1983**, *16*, 1607.

MA000261T